IEEE Robotics and Automation Letters (RA-L) paper, presented at ICRA 2024, Yokohama, Japan. Cite as RA-L paper.

Seamless Reaction Strategy for Bipedal Locomotion Exploiting Real-Time Nonlinear Model Predictive Control

JongHun Choe[1], Joon-Ha Kim[1], Seungwoo Hong[1],
Jinoh Lee[2], *Senior Member, IEEE* and Hae-Won Park[1], *Member, IEEE*

***Abstract*—This paper presents a reactive locomotion method for bipedal robots enhancing robustness and external disturbance rejection performance by seamlessly rendering several walking strategies of the ankle, hip, and footstep adjustment. The Nonlinear Model Predictive Control (NMPC) is formulated to take into account nonlinear Divergent Component of Motion (DCM) error dynamics that predicts the future states of the robot in response to the walking strategies. This formulated NMPC enables the seamless application of these strategies improving push disturbance rejection performance. The proposed controller is validated in simulation and through an experiment on a bipedal robot platform, Gazelle, which confirms its effectiveness in real-time.**

***Index Terms*—Legged Robots, Humanoid and Bipedal Locomotion, Optimization and Optimal Control**

I. Introduction

BIPEDAL robots, also known as humanoids, gain attention for their potential to navigate various environments that conventional wheeled robots cannot [1]. To reach this potential, a key milestone is to achieve versatile and stable walking abilities comparable to human performance. One effective method for bipedal robots to walk is pattern-based walking, in which a pre-computed walking pattern is generated using a simplified model [2], [3] of the robot, and the robot follows the Center of Mass (COM) and foot trajectory. However, this method is prone to disturbances and modeling errors. To mimic human walking performance, the robot should possess human-level stability and the ability to react robustly to disturbances.

Humans use various strategies such as *ankle, hip,* and *stepping strategies* to overcome unexpected disturbances [4]–[6], and utilize all walking strategies simultaneously and adapt their choice of strategy based on the situation and condition. The ankle strategy generates ankle torque against external pushes, the hip strategy creates counter momentum concerning the body angular acceleration, and the stepping strategy adjusts the swing foots landing position and the overall footstep periods. In the case of robots, the ankle and hip strategies change the point of the stance foot where the ground reaction force is focused, and the stepping strategy adjusts the reference footstep position and footstep time of the swinging leg. To emulate human-like fine locomotion ability, it is necessary for robots to be able to seamlessly incorporate all walking strategies in their movements. However, it is challenging to compute overall control inputs corresponding to each strategy at once while considering the constraints, such as the physical limitation of the robots and robot model dynamics.

In this study, Model Predictive Control (MPC) is utilized, one of the optimization-based control frameworks that predict the robots future state with the dynamics and obtains the control inputs that minimize the user-defined costs during a fixed time horizon. Authors in [7]–[13] applied the MPC to bipedal robot walking and showed impressive results in walking and disturbance rejection performance. Moreover, with the MPC method, there are examples that present the method to use either one or two strategies on the bipedal robot selectively [14], [15]. Recently, studies have been presented that implement all strategies mentioned above sequentially [8]–[10], [16]. Authors in [9] have demonstrated the successful implementation of all strategies on a real bipedal robot, achieving impressive performance. However, linear approximations and sequential usage of the ankle strategy in a specific order are utilized to formulate the problem into a Quadratic Programming (QP) problem. In this sequential usage, the ankle strategy is always applied first, followed by other strategies in response to the disturbance, resulting in the less flexible use of each strategy. Moreover, authors in [12], [13] have presented a Nonlinear MPC (NMPC) framework that considered ankle, hip, footstep position change, and COM height variation strategies. They use a various-height inverted pendulum model and successfully verify their algorithm for disturbance rejection in the simulation environment, but they do not consider the footstep time change strategy. Recently, authors in [17], [18] have presented research on detecting walkable areas using vision sensors on a humanoid robot and generating walking patterns for traversing those areas. When modifying the patterns for the walkable areas, the strategies mentioned above are sequentially applied, and their methods are validated through hardware experiments.

Although the use of MPC for walking strategies has shown promising results in controlling bipedal robots, incorporating

Manuscript received: March, 6, 2023; Revised May, 22, 2023; Accepted June, 19, 2023.

This paper was recommended for publication by Editor Abderrahmane Kheddar upon evaluation of the Associate Editor and Reviewers' comments. This work was supported in part by Korea Evaluation Institute of Industrial Technology (KEIT) funded by the Korea Government (MOTIE) under Grant No.20018216, Development of mobile intelligence SW for autonomous navigation of legged robots in dynamic and atypical environments for real application.

[1]Authors are with the Humanoid Robot Research Center, School of Mechanical, Aerospace & Systems Engineering, Department of Mechanical Engineering, Korea Advanced Institute of Science and Technology (KAIST), Yuseong-gu, 34141 Daejeon, Republic of Korea. haewonpark@kaist.ac.kr

[2]Author is with the Institute of Robotics and Mechatronics, German Aerospace Center (DLR), 82234 Weßling, Germany, and is also an adjunct professor at the Department of Mechanical Engineering, Korea Advanced Institute of Science and Technology (KAIST), Yuseong-gu, 34141 Daejeon, Republic of Korea.

Digital Object Identifier (DOI): see top of this page.

IEEE Robotics and Automation Letters (RA-L) paper, presented at ICRA 2024, Yokohama, Japan. Cite as RA-L paper.

IEEE Robotics and Automation Letters (RA-L) paper, presented at ICRA 2024, Yokohama, Japan. Cite as RA-L paper.

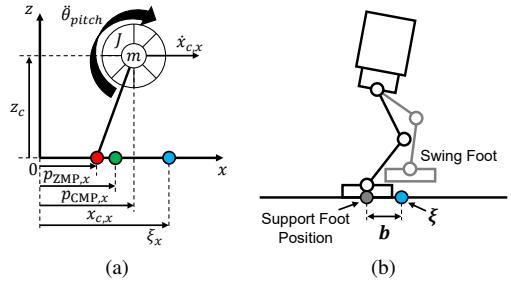

(a) (b)

Fig. 1. (a): Illustration of LIPFM and DCM dynamics. $\ddot{\theta}_{pitch} \in \mathbb{R}$ means the robot body angular acceleration in the pitch direction, (b): Corresponding sagittal view of the robot.

multiple strategies in a seamless manner while considering the robot's physical limitations and dynamics remains a challenge. Therefore this paper proposes a method in which the bipedal robot can overcome the disturbance with a seamless reaction by considering ankle, hip, and stepping strategies simultaneously. The control inputs, representing the reaction strategies, are calculated through the optimal control problem based on pattern-based walking. Taking into account the Linear Inverted Pendulum with Flywheel Model (LIPFM) dynamics and the relationship between the error of Divergent Component of Motion (DCM) [14]–[16], [19]–[21] and the strategies, the NMPC method is employed. To implement the proposed NMPC method on actual bipedal robot hardware, the problem must be solved in real-time. Accordingly, this paper strives to make the following specific contributions:

- formulation of an NMPC problem to bring seamless ankle, hip, and stepping reaction strategies into bipedal locomotion which effectively overcomes disturbances;
- implementation of the proposed NMPC method on 13 Degrees-of-Freedom (DOF) bipedal robot in real-time which has rarely been found with a real hardware setup.

The remainder of this paper is organized as follows: Sec. II introduces the backgrounds of this study. Sec. III states the problem this study intends to solve and addresses the NMPC framework proposed in this study. Sec. IV verifies the proposed controller through simulation, and experimental results obtained using actual bipedal robot hardware is presented in Sec. V. Finally, Section VI draws a conclusion.

II. Background

This section provides an overview of the simplified model of the robot and the DCM [14]–[16], [19]–[21].

A. Robot Model Dynamics

The schematic diagram of LIPFM is shown in Fig. 1 (a). $\boldsymbol{p}_{\text{ZMP}} \in \mathbb{R}^2$ means the position of the ZMP in x, y directions, and $\boldsymbol{p}_{\text{CMP}} \in \mathbb{R}^2$ represents the Centroidal Momentum Pivot (CMP) [15], [22] in x, y directions. $\boldsymbol{x}_c \in \mathbb{R}^2$ indicates the position of COM in x, y directions, and $\ddot{\boldsymbol{\theta}} \in \mathbb{R}^2$ denotes the angular acceleration of the robot body in pitch and roll directions. $\boldsymbol{J} \in \mathbb{R}^{2\times 2}$ denotes the rotational inertia of the robot body, which has pitch and roll value as its diagonal element. Assuming that the vertical height of COM is constant, the governing equation of the LIPFM is as follows:

$$\ddot{\boldsymbol{x}}_c = \omega^2(\boldsymbol{x}_c - \boldsymbol{p}_{\text{CMP}}), \quad \boldsymbol{p}_{\text{CMP}} = \boldsymbol{p}_{\text{ZMP}} + \boldsymbol{J}\ddot{\boldsymbol{\theta}}/mg, \quad (1)$$

where ω is the natural frequency of the robot defined by $\sqrt{g/z_c}$, m is the total mass of the robot, and g is the acceleration of gravity.

B. DCM Error Equation

1) Divergent Component of Motion: It is derived from the COM position and velocity with a simplified model such as LIPFM. It states where the robot's foot should land at the end of the step for the robot to come to a complete stop. The DCM $\boldsymbol{\xi}$ can be expressed as follows:

$$\boldsymbol{\xi} = \boldsymbol{x}_c + \dot{\boldsymbol{x}}_c/\omega, \quad (2)$$

where $\boldsymbol{\xi} \in \mathbb{R}^2$ denotes the DCM in x, y directions, and $\dot{\boldsymbol{x}}_c \in \mathbb{R}^2$ denotes the COM velocity in x, y directions. With the pre-planned footsteps, the COM reference trajectory of the robot can be generated by various pattern-based walking algorithms. Because this trajectory includes position and velocity information of the COM, the DCM reference trajectory can also be calculated from the gait pattern using (2).

According to its definition, if the robot steps on to the DCM, the robot will come to a stop. Therefore, for walking with the desired speed, the support foot position of the robot should locate with offset vector $\boldsymbol{b} \in \mathbb{R}^2$ in x, y directions (see Fig. 1 (b)), which we call DCM offset hereafter, with respect to the distance between the DCM and the position of the foot at the end of step [16].

It is known that when $\boldsymbol{h}^{\max} \in \mathbb{R}^2$ are the maximum foot strides of the gait pattern in x, y direction, and the minimum footstep time is $T^{\min}$, the maximum value of the DCM offset in x, y direction for stable locomotion are express as $\boldsymbol{b}^{\max} = \boldsymbol{h}^{\max}/(e^{\omega T^{\min}} - 1)$ [23]. Similar to DCM and COM, the reference value of DCM offset $\boldsymbol{b}^{ref}$ is included in the gait pattern and obtained from various pattern-based walking algorithms. When stepping strategies are employed, the DCM offset value will be changed at each step from the reference value according to the choice of footstep position change ($\boldsymbol{\delta u} \in \mathbb{R}^2$), and the variable ($\boldsymbol{\delta b} \in \mathbb{R}^2$) will represent this change.

2) Relationship between the DCM Error and Walking Strategies: A carefully generated pre-defined gait pattern including the COM and DCM reference trajectory can be used for stable locomotion with the assumption that the robot follows the LIPFM dynamics. However, in response to external pushes and the modeling gap between LIPFM dynamics and a real robot, the actual DCM may deviate from the DCM reference trajectory, thereby creating errors between the actual DCM and DCM reference. In this study, we use various walking strategies to handle this DCM error. The relationship

IEEE Robotics and Automation Letters (RA-L) paper, presented at ICRA 2024, Yokohama, Japan. Cite as RA-L paper.

between the DCM error and various walking strategies is given by the following equation proposed in [9]:

$$\boldsymbol{\delta u}+\boldsymbol{\delta b}+\boldsymbol{\xi}^{ref}e^{\omega({}^kT^{ref}-t)}(1-e^{\omega\delta T})+(e^{\omega({}^kT^{ref}+\delta T-t)}-1)\frac{\boldsymbol{J\ddot{\theta}}}{mg}$$
$$=(\boldsymbol{\xi}^{err}-(\boldsymbol{p}_{\text{c,ZMP}}+\frac{\boldsymbol{J\ddot{\theta}}}{mg}))e^{\omega({}^kT^{ref}+\delta T-t)}+\boldsymbol{p}_{\text{c,ZMP}}+\frac{\boldsymbol{J\ddot{\theta}}}{mg}, \tag{3}$$

where t is the time that resets to zero at the start of every footstep, and k is the current footstep number. $\boldsymbol{\xi}^{err} \in \mathbb{R}^2$ and $\boldsymbol{\xi}^{ref} \in \mathbb{R}^2$ represent the DCM error and the reference DCM value in x, y directions, respectively, while $\boldsymbol{p}_{\text{c,ZMP}} \in \mathbb{R}^2$ is the control ZMP [24] in x, y directions, which is the variable that the robot can change within a limited range (usually the size of the foot) using the ankle torque. The relationship between $\boldsymbol{p}_{\text{c,ZMP}}$ and $\boldsymbol{p}_{\text{ZMP}}$ is expressed as $\boldsymbol{p}_{\text{ZMP}} = \boldsymbol{u} + \boldsymbol{p}_{\text{c,ZMP}}$, where $\boldsymbol{u}$ represents the position of the support foot. ${}^kT^{ref}$ is the reference footstep time at k^{th} footstep, and δT means the footstep time change. Notice that (3) has a nonlinear relationship among the DCM error ($\boldsymbol{\xi}^{err}$), ankle strategy ($\boldsymbol{p}_{\text{c,ZMP}}$), stepping strategies ($\boldsymbol{\delta u}$, δT), and hip strategy ($\boldsymbol{\ddot{\theta}}$).

III. Method

This section describes the NMPC problem that the proposed controller aims to solve.

A. Problem Statement

Fig. 2 shows the sequence of how the bipedal robot overcomes disturbances by utilizing (3) while following a pre-defined gait pattern. ${}^k\boldsymbol{u}^{ref} \in \mathbb{R}^2$ is the reference footstep position at the k^{th} footstep in the x, y direction. When there is no disturbance, the CMP is located at its reference value $\boldsymbol{p}^{ref}_{\text{CMP}}$ from the pre-defined pattern, and the DCM diverges from the CMP as time goes on.

Next, Fig. 2 illustrates the cases when a disturbance occurs while the robot follows a pre-defined pattern. The DCM affected by the disturbance is expressed as $\boldsymbol{\xi} := \boldsymbol{\xi}^{ref} + \boldsymbol{\xi}^{err}$. The reference DCM ($\boldsymbol{\xi}^{ref}$) is computed from a pre-defined pattern, which is driven by the *preview control* [25]. Fig. 2 (a) shows the case when the robot does not employ any walking strategies. The DCM offset at the end of the footstep ($\boldsymbol{b}_{{}^kT^{ref}} \in \mathbb{R}^2$) is significantly changed from its reference value ($\boldsymbol{b}^{ref}_{{}^kT^{ref}} \in \mathbb{R}^2$). If $\boldsymbol{b}_{{}^kT^{ref}}$ exceeds the limit calculated above, the robot will eventually fall.

To avoid falling while maintaining the pre-defined gait pattern, the walking strategies should be effectively applied to reduce the DCM error $\boldsymbol{\xi}^{err}$. These strategies are exemplified in Fig. 2 (b). When a DCM error occurs, the ankle strategy adjusts the control ZMP ($\boldsymbol{p}_{\text{c,ZMP}}$) in (3), and the hip strategy generates body angular accelerations ($\boldsymbol{\ddot{\theta}}$). The resultant CMP, represented as $\boldsymbol{p}_{\text{CMP}}$, is calculated as the sum of the reference footstep position, control ZMP, and body angular acceleration. The DCM error at the end of the footstep can be reduced by adjusting the footstep position and timing. The footstep position change is a sub-strategy of the stepping strategy, which generates $\boldsymbol{\delta u}$ in (3). Changing the footstep time, represented as δT in (3), is another way to lower the DCM error. The DCM error can also be reduced by generating a DCM offset change ($\boldsymbol{\delta b}$ in (3)). Therefore, the proposed NMPC controller is designed to suppress the occurrence of the DCM offset as much as possible.

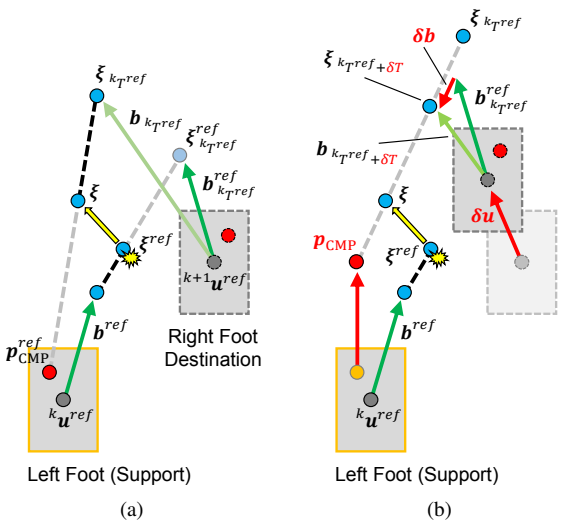

Fig. 2. Graphical diagrams of (a) original walking pattern when the disturbance occurs, and (b) the proposed control method overcoming the disturbance with ankle, hip, and stepping strategies.

Within the LIPFM dynamics assumption, the relationship between each strategy's free variables and the DCM error can be expressed as (3). However, more than one combination of these variables can exist, and their relationship forms with high nonlinearity. For this reason, the previous studies solve the problem sequentially for the ankle strategy first and then other strategies [9]. Additionally, linearization approximations, such as the footstep time change, are often used in the stepping strategy. In contrast, this study defines the problem as an NMPC problem and solves it using a nonlinear optimization solver. As a result, without the sequential approach and the linearization approximations, ankle ($\boldsymbol{p}_{\text{c,ZMP}}$), hip ($\boldsymbol{\ddot{\theta}}$), and stepping ($\boldsymbol{\delta u}$, δT) strategies are seamlessly amalgamated and their weightings are intuitively adjustable by setting user-tuned weighting factors in the cost functions of the optimal control problem.

B. Optimal Control Problem

1) Optimization Variables: When the horizon of the NMPC problem is H, the optimization variables used in this study consist of states $\boldsymbol{\xi}^{err}_i$ for the time step $i = 0, 1, \cdots, H$, and the control inputs $\boldsymbol{v}_i$ which are given by

$$\boldsymbol{v}_i = [\boldsymbol{p}^T_{\text{c,ZMP},i}\ \boldsymbol{\delta u}^T_i\ \boldsymbol{\delta b}^T_i\ \delta T_i\ \boldsymbol{\ddot{\theta}}^T_i]^T, \quad (i = 0, \cdots, H-1).$$

Note that in this study, the time step i denotes the variable in the NMPC problem.

2) Cost Function: With the optimization variables defined in the previous subsection, the cost function of the proposed

IEEE Robotics and Automation Letters (RA-L) paper, presented at ICRA 2024, Yokohama, Japan. Cite as RA-L paper.

NMPC problem is defined as follows to reduce DCM error and control inputs:

$$J = \sum_{i=1}^{H} (\boldsymbol{\xi}_i^{err})^T \boldsymbol{Q} (\boldsymbol{\xi}_i^{err}) + \sum_{i=0}^{H-1} (\boldsymbol{v}_i)^T \boldsymbol{R} (\boldsymbol{v}_i), \tag{4}$$

where $\boldsymbol{Q}$ and $\boldsymbol{R}$ denote the weight matrices of the states and control inputs, respectively, and those are defined as

$$\begin{aligned} \boldsymbol{Q} &= \mathrm{diag}(\omega_{\xi_x^{err}}, \omega_{\xi_y^{err}}) \\ \boldsymbol{R} &= \mathrm{diag}(\omega_{p_{\mathrm{c,ZMP},x}}, \omega_{p_{\mathrm{c,ZMP},y}}, \omega_{\delta u_x}, \omega_{\delta u_y}, \\ &\qquad \omega_{\delta b_x}, \omega_{\delta b_y}, \omega_{\delta T}, \omega_{\ddot{\theta}_{pitch}}, \omega_{\ddot{\theta}_{roll}}), \end{aligned}$$

where $\mathrm{diag}()$ represents the diagonal matrix, and ω_j denotes the weighting factor of the optimization variable j.

3) Equality Constraints: Two equality constraints are considered in the proposed NMPC problem. First is the DCM error dynamics equality constraint, derived from the LIPFM dynamics. Using (1) and (2), the dynamic relationship between the DCM and the CMP of the robot can be expressed as $\dot{\boldsymbol{\xi}}_i = \omega(\boldsymbol{\xi}_i - \boldsymbol{p}_{\mathrm{CMP},i})$. Furthermore, assuming that the DCM pattern does not violate the LIPFM dynamics, the reference part can be removed as follows:

$$\dot{\boldsymbol{\xi}}_i^{err} = \omega(\boldsymbol{\xi}_i^{err} - (\boldsymbol{p}_{\mathrm{c,ZMP},i} + \boldsymbol{J}\ddot{\boldsymbol{\theta}}_i / mg)). \tag{5}$$

Now by discretizing (5), the relationship of DCM error between the time step i and $i+1$ can be derived as follows:

$$\begin{aligned} \boldsymbol{\xi}_{i+1}^{err} - (1 + \omega \Delta t^{MPC}) \boldsymbol{\xi}_i^{err} + \omega \Delta t^{MPC} \boldsymbol{p}_{\mathrm{c,ZMP},i} \\ + \omega \Delta t^{MPC} \frac{\boldsymbol{J}\ddot{\boldsymbol{\theta}}_i}{mg} = \boldsymbol{0}, \end{aligned} \tag{6}$$

where Δt^{MPC} denotes the sampling time of the proposed NMPC problem. Moreover, unless otherwise specified, the remaining constraints of the proposed NMPC problem are defined for $i = 0, \cdots, H-1$.

Next, (3) is modified and added as another equality constraint to consider the relationship between the DCM error and variables changed by the walking strategies. With control inputs $\boldsymbol{v}_i$, (3) can be expressed as follows:

$$\begin{aligned} \boldsymbol{\delta u}_i + \boldsymbol{\delta b}_i + \boldsymbol{\xi}_i^{ref} e^{\omega({}^k T^{ref} - t_i)} (1 - e^{\omega \delta T_i}) - \boldsymbol{p}_{\mathrm{c,ZMP},i} - \frac{2\boldsymbol{J}\ddot{\boldsymbol{\theta}}_i}{mg} \\ - (\boldsymbol{\xi}_i^{err} - (\boldsymbol{p}_{\mathrm{c,ZMP},i} + \frac{2\boldsymbol{J}\ddot{\boldsymbol{\theta}}_i}{mg})) e^{\omega({}^k T^{ref} + \delta T_i - t_i)} = \boldsymbol{0}. \end{aligned} \tag{7}$$

Notice that the relationship between the DCM error and the control inputs in (7) is highly nonlinear. To construct and solve the optimization problem with above nonlinear constraints, NMPC method should be utilized.

4) Inequality Constraints: Inequality constraints are set to consider the physical limitations of the robot. Because the control ZMP cannot be outside of the robot's foot, the control ZMP should satisfy the following inequality:

$$|p_{\mathrm{c,ZMP},x,i}| \leq l_{F,x}/2, \quad |p_{\mathrm{c,ZMP},y,i}| \leq l_{F,y}/2, \tag{8}$$

where $l_{F,x}$ and $l_{F,y}$ denote the foot size in x and y directions, respectively (generally foot length and width).

The swing foot should land within the range of the leg's workspace, and body angular acceleration should be bounded, which is prescribed as

$$-\boldsymbol{\delta u}^{\max} \leq \boldsymbol{\delta u}_i \leq \boldsymbol{\delta u}^{\max}, \quad -\ddot{\boldsymbol{\theta}}^{\max} \leq \ddot{\boldsymbol{\theta}}_i \leq \ddot{\boldsymbol{\theta}}^{\max}. \tag{9}$$

Next, the change of the footstep time δT_i are set with the minimum and maximum values as follows:

$$\delta T^{\min} \leq \delta T_i \leq \delta T^{\max}, \tag{10}$$

which is determined by users with respect to the nominal footstep time ${}^k T^{ref}$ from the pre-defined pattern.

Finally, footstep position change is regulated by maximum foot speed as below:

$$-\dot{\boldsymbol{u}}^{\max} \Delta t \leq \boldsymbol{\delta u}_0 - \boldsymbol{\delta u}^{prev} \leq \dot{\boldsymbol{u}}^{\max} \Delta t, \tag{11}$$

$$-i\dot{\boldsymbol{u}}^{\max} \Delta t^{MPC} \leq \boldsymbol{\delta u}_i - \boldsymbol{\delta u}^{prev} \leq i\dot{\boldsymbol{u}}^{\max} \Delta t^{MPC}, \tag{12}$$

where $\dot{\boldsymbol{u}}^{\max} \in \mathbb{R}^2$ denotes maximum foot speed in x, y-directions, Δt denotes the controller sampling time, and $\boldsymbol{\delta u}^{prev}$ denotes the footstep position change determined at the previous control loop.

With the optimization variables ($\boldsymbol{\xi}_i^{err}$, $\boldsymbol{v}_i$), cost function (4), equality constraints (6), (7), and inequality constraints (8)-(12), the proposed NMPC problem is formulated. The formulated NMPC problem is solved using the Sequential Quadratic Programming (SQP) method with the implementation of the QP solver [26] to solve a sub-QP problem. The sub-QP problem is formulated using quadratic approximation of the cost function and linear approximation of the constraints. The quadratic approximation of the cost function can be obtained using the gradient and Hessian of the cost function, and linear approximation of the constraints requires the gradients of constraints. The gradient and Hessian of the cost function, and gradients of constraints are computed with CasADi [27]. The description of the SQP method used in this study is omitted for the sake of brevity (please refer to [28] for further details.)

The control inputs obtained from the NMPC problem are applied to the robot as follows. Body angular acceleration is directly applied to adjust the orientation of the robot's body, and the control ZMP is converted into ankle torque. Step position change and step time change are utilized to modify the desired destination of the swing foot. As a result, overall joint angles are calculated with inverse kinematics by considering the updated swing foot's destination and the modified body orientation.

IV. Numerical Analysis and Verification

This section presents the results of evaluating the proposed controller, which can seamlessly incorporate various walking strategies. To compare its performance against an existing controller, a framework from [9] is used as a baseline. The LIPFM model is employed for the robot model, and all simulations are conducted using the MATLAB environment[1]. The parameters and weighting factors used in the proposed controller are shown in Table I, while a horizon length of $H = 15$ and a sampling time of $\Delta t^{MPC} = 0.025\ s$ are set.

[1]The simulation code is released at https://github.com/DrcdKAIST/Gazelle_NMPC_controller/

IEEE Robotics and Automation Letters (RA-L) paper, presented at ICRA 2024, Yokohama, Japan. Cite as RA-L paper.

TABLE I
WEIGHTING FACTORS AND PARAMETERS USED IN SIMULATIONS AND EXPERIMENTS

Weighting factor	$\omega_{\xi_x^{err}}$	$\omega_{\xi_y^{err}}$	$\omega_{p_{\text{c,ZMP},x}}$	$\omega_{p_{\text{c,ZMP},y}}$	$\omega_{\delta u_x}$	$\omega_{\delta u_y}$	$\omega_{\delta b_x}$	$\omega_{\delta b_y}$	$\omega_{\delta T}$	$\omega_{\ddot{\theta}_{pitch}}$	$\omega_{\ddot{\theta}_{roll}}$
Flat foot	1	1	10	50	1	10^2	10^3	10^3	10^2	10^{-2}	10^{-1}
Point foot	10	10	-	-	1	10	10^5	10^5	10^2	10^{-1}	10^{-1}
Fig. 5 Ankle strategy	10	1	1	50	10	10^2	10^2	10^3	10	10	10^{-1}
Fig. 5 Hip strategy	10	1	50	50	10	10^2	10^2	10^3	10	10^{-3}	10^{-1}
Fig. 5 Stepping strategy (footstep position change)	10	1	5×10^2	50	10^{-1}	10^2	10^2	10^3	10	10	10^{-1}
Fig. 5 Stepping strategy (footstep time change)	10	1	2×10^2	50	10	10^2	10^2	10^3	1	10	10^{-1}
Experiment	1	1	1	1	10	10	10^3	10^3	10^2	-	-

Parameter	$l_{F,x}$	$l_{F,y}$	$\delta u_x^{\max}$	$\delta u_y^{\max}$	$\ddot{\theta}_{pitch}^{\max}$	$\ddot{\theta}_{roll}^{\max}$	$\delta T^{\max}$	$\delta T^{\min}$	$\dot{u}_x^{\max}$	$\dot{u}_y^{\max}$
Simulation	0.18 m	0.13 m	0.3 m	0.2 m	1000 deg/s^2	1000 deg/s^2	0.0 s	-0.2 s	0.7 m/s	0.6 m/s
Experiment	0.16 m	0.10 m	0.3 m	0.2 m	-	-	0.05 s	-0.05 s	0.7 m/s	0.6 m/s

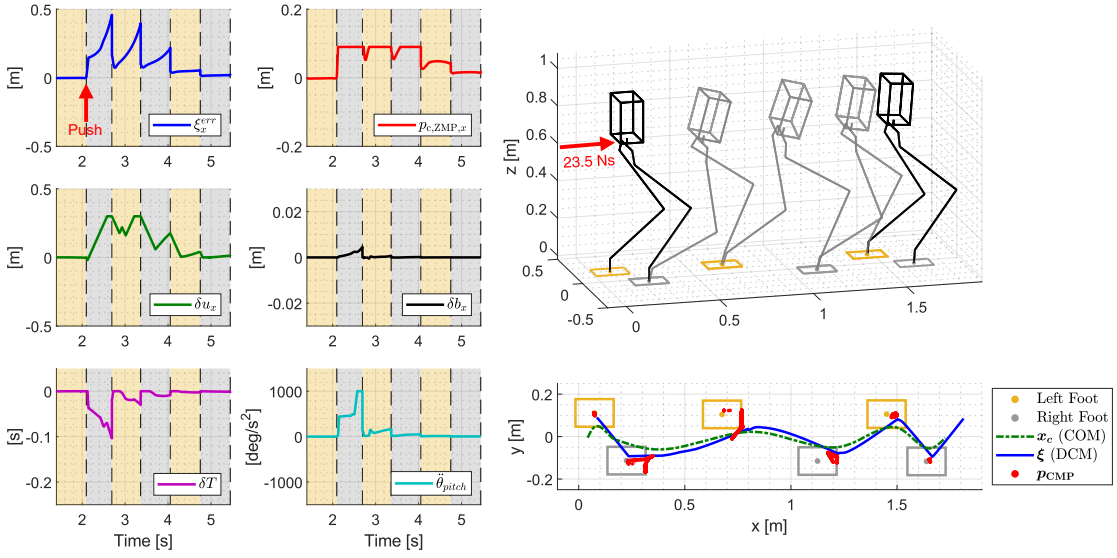

(a) Forward push (23.5 Ns, duration: 0.05 s)

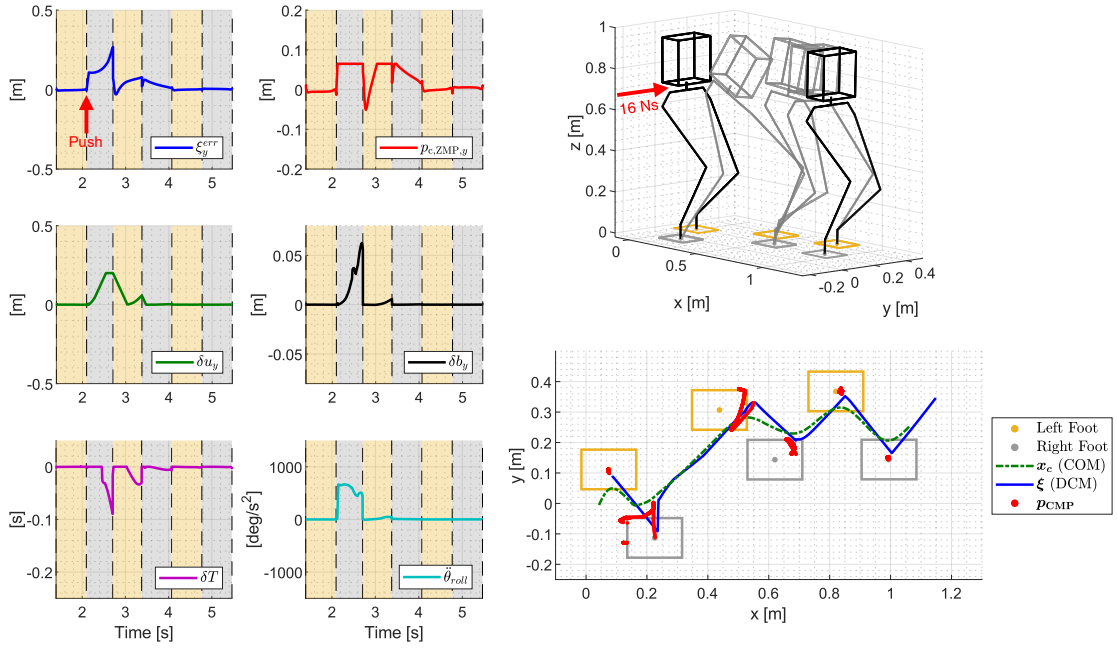

(b) Side push (16 Ns, duration: 0.05 s)

Fig. 3. The result of the forward- and side-push recovery simulations, where the robot initially walks forward with 0.15 m footstep stride and 0.7 s footstep time, and the disturbance is applied at the beginning of 2^{nd} step, 2.1 s. Left-side plots show the DCM error, $\boldsymbol{\xi}^{err}$, and the following control inputs: control ZMP, $\boldsymbol{p}_{\text{c,ZMP}}$, footstep position change, $\boldsymbol{\delta u}$, DCM offset change, $\boldsymbol{\delta b}$, footstep time change, δT, and body angular acceleration, $\ddot{\boldsymbol{\theta}}$. Right-side plots present the robot's reaction to the disturbance.

IEEE Robotics and Automation Letters (RA-L) paper, presented at ICRA 2024, Yokohama, Japan. Cite as RA-L paper.

IEEE Robotics and Automation Letters (RA-L) paper, presented at ICRA 2024, Yokohama, Japan. Cite as RA-L paper.

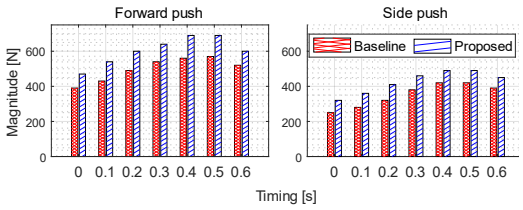

Fig. 4. The plots of the maximum magnitude of disturbance (y-axis) the robot can overcome, depending on the timing of the disturbance (x-axis) for forward push on the left and side push on the right, respectively.

A. Push Recovery Simulations

Fig. 3 demonstrates how the bipedal robot model overcomes disturbances while walking with the proposed controller. The left-side plots show the DCM error and the control inputs gernerated to compensate for the error, and the right-side plot shows the robot's reaction to the disturbance. The seamless response of the proposed method can be seen in the control inputs of all strategies appearing simultaneously. Furthermore, unlike the baseline controller, other strategies such as hip and stepping strategies are activated even if the robot does not fully utilize the ankle torque. One can also observe that control inputs of the hip and stepping strategies ($\ddot{\boldsymbol{\theta}}, \boldsymbol{\delta u}, \delta T$) appear when the ankle strategy's control input ($\boldsymbol{p}_{c,\mathrm{ZMP}}$) does not reach its limitation.

In these simulations, the robot model initially walks with a stride of 0.15 m and a period of 0.7 s. A disturbance is applied at the beginning of the 2^{nd} footstep. In Fig. 3, the model's left foot is depicted in yellow, and the right foot is colored gray. The colored zones indicate the support phase of the corresponding foot, and the width of each area represents the footstep time of the support foot in the left graphs of Fig. 3. The figure shows the robot model overcoming both forward and side pushes while walking. In the forward push case, the disturbance is 23.5 Ns with a magnitude of 470 N and a duration of 0.05 s, and in the side push case, the robot model

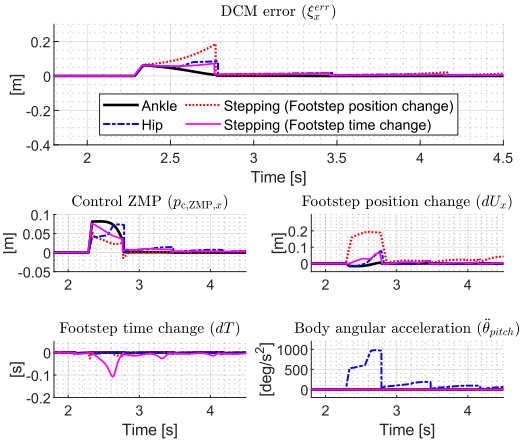

Fig. 5. The forward-push recovery simulation results with different reaction strategies (ankle, hip, and footstep position/time) flexibly chosen by changing the combination of the weighing factors of the proposed method.

overcomes 16 Ns of disturbance with a magnitude of 320 N and a duration of 0.05 s. Both cases demonstrate that the robot model successfully overcomes the disturbance.

In Fig. 4, we further investigate the maximum disturbance magnitudes tolerated by controllers when the magnitude and timing of the external push are changed over the entire walking period. The robot model initially walks with a stride of 0.15 m and a footstep time of 0.7 s. The external pushes are then applied at every time interval of 0.1 s by increasing the magnitude by 10 N. One can observe that the proposed seamless approach enables the robot model to mitigate larger disturbances effectively at all points.

Fig. 5 shows the flexibility of the proposed method through a number of forward-push recovery simulations with combinations of the weighing factors while maintaining a consistent disturbance magnitude, duration, and timing. The robot model initially walks in place with a footstep time of 0.7 s, and

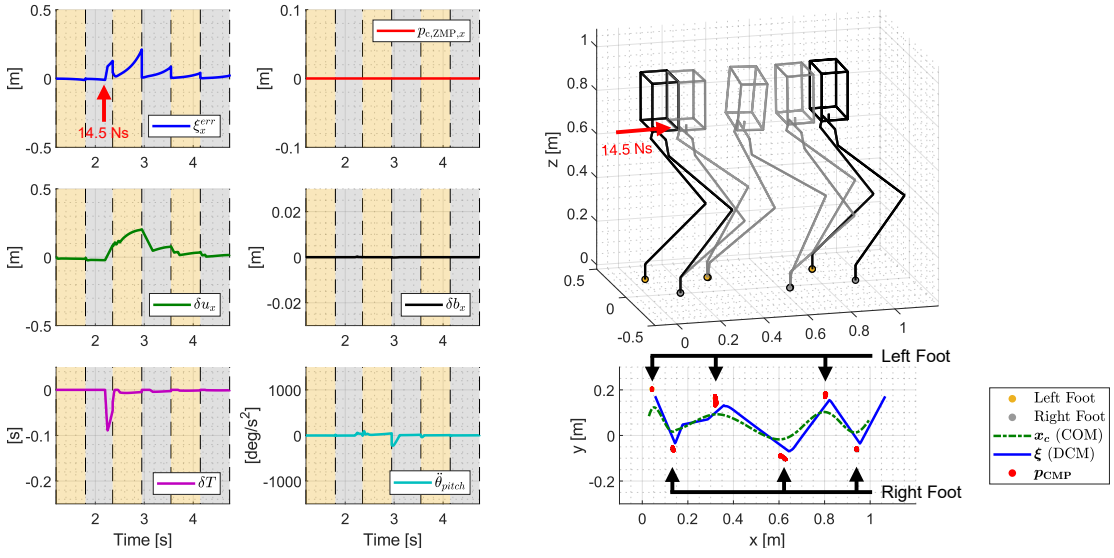

Fig. 6. The result of the push recovery simulation with the point foot robot model, where the robot walks with 0.1 m stride length, and 0.6 s footstep time. The disturbance of 14.5 Ns with 0.05 s duration is applied at 0.4 s of the 2^{nd} footstep, i.e., t= 2.199 s. The upper-right figure shows the robot's reaction as time goes on, and its top view is shown in the lower-right corner. DCM error and corresponding control inputs are displayed in the left graphs.

IEEE Robotics and Automation Letters (RA-L) paper, presented at ICRA 2024, Yokohama, Japan. Cite as RA-L paper.

IEEE Robotics and Automation Letters (RA-L) paper, presented at ICRA 2024, Yokohama, Japan. Cite as RA-L paper.

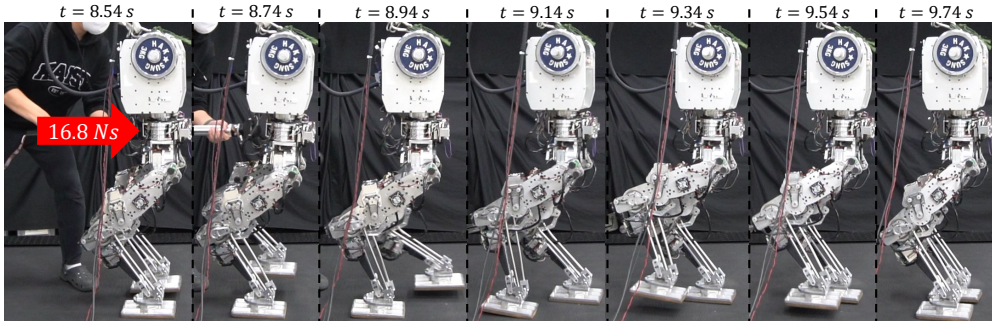

Fig. 7. Snapshots of the reaction against the sudden disturbance while walking in place at 8.54s, measured as 16.8Ns with the maximum impact force of 348.1N and impact time duration of 0.174s.

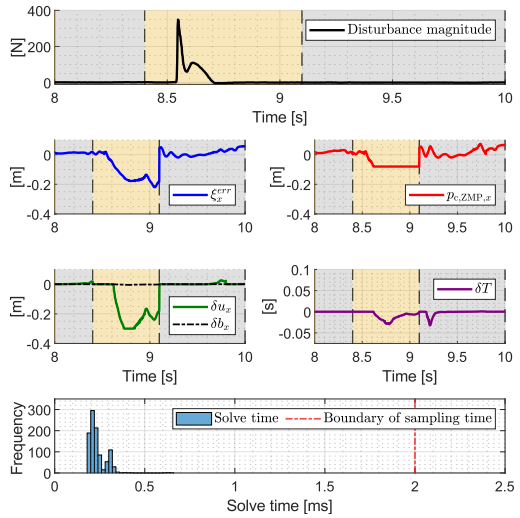

Fig. 8. Results of the actual bipedal robot experiment: (top) the push force which is measured with a force sensor; (middle)the DCM error and control inputs such as control ZMP, footstep position change, and footstep time change; (bottom) the histogram of NMPC solve time during the experiment.

the disturbance is 10 Ns with a magnitude of 200 N and a duration of 0.05 s. The parameters and weighting factors used in this simulation are shown in Table I, except for the maximum x direction foot speed ($\dot{u}_x$), which is increased to 2.0 m/s to improve the representation of footstep position change. Fig. 5 demonstrates that the utilization of the strategies can be flexibly selected by selecting the appropriate combination of weighting factors.

To emphasize the effectiveness of the stepping strategy with the footstep time change, forward push recovery simulation is conducted under the same conditions as Fig. 3 (a), except the upper (δT^{max}) and lower boundaries (δT^{min}) of the footstep time change are set to zero. Under these conditions, the robot model cannot recover from the 23.5 Ns disturbance and can overcome a maximum of 20.5 Ns with a magnitude of 410 N and duration of 0.05 s, resulting in a 13.6 % decrease. Therefore, the push recovery performance can be improved by applying the stepping strategy with the footstep time change.

B. Push Recovery with a Point-Foot Bipedal Robot Model

The proposed controller seamlessly incorporates all walking strategies, making it applicable to a wide range of bipedal robots, regardless of their shape. For instance, the point foot robot, which has no ankle, can still demonstrate the effectiveness of the proposed method. Since the point foot robot only makes contact with the ground using a "point", the ankle strategy is not available. However, even in this under-actuated situation, the proposed controller can maintain the balance and successfully perform push recovery, showing its robustness and wider applicability.

Fig. 6 shows the response of a point foot robot model that overcomes a forward push while walking with the proposed controller. In the simulation, the robot model is pushed at 0.4 s of the second footstep, while the robot model is walking with a stride length of 0.1 m and a footstep time of 0.7 s. The 14.5 Ns of the disturbance is applied to the robot model, with 290 N of magnitude and 0.05 s of duration. The weighting factors and the parameters of the controller are shown in Table I, while the foot size is set to zero because the robot model has the point foot.

The left side plots of Fig. 6 present the DCM errors caused by the disturbance and the control inputs created to compensate for it. The figure illustrates that all control inputs, except for the control ZMP ($\boldsymbol{p}_{\mathrm{c,ZMP}}$), are simultaneously utilized to balance the robot model. The control ZMP is always zero, indicating that the robot model does not use the ankle strategy at all.

V. EXPERIMENT

In this section, we describe the application of the proposed NMPC method to a real bipedal robot, Gazelle [29]. The controller is implemented on the PC with a processor up to 3.50 GHz speed for adequate computational power. As a QP solver, qpSWIFT [26] is utilized to solve the NMPC problem, and the maximum SQP iteration number is limited to 3 for achieving real-time conditions. We set the horizon length to $H = 10$, and the sampling time for the NMPC controller is $\Delta t^{MPC} = 0.025$ s, while the overall robot operates at a sampling time of $\Delta t = 0.002$ s. The values for weighting factors and parameters used in the NMPC are listed in Table I. The control ZMP is converted into foot force using the ZMP distributor [30]. Moreover, the velocity of the ankle joint is calculated that minimizes the difference between the converted foot force and the measured value using the ankle torque sensor.

IEEE Robotics and Automation Letters (RA-L) paper, presented at ICRA 2024, Yokohama, Japan. Cite as RA-L paper.

Figs. 7 and 8 show the robot's response to a disturbance and its experimental results. The robot is walking in place with a footstep time of 0.7 s when it is pushed with a rod. A force sensor is attached to the end of the rod to measure the push force. The top graph of Fig. 8 depicts the push force applied to the robot. The maximum impact force is 348.1 N, and the total duration of the disturbance is 0.174 s.

The robot employs strategies to counteract the external push, such as ankle and footstep position and footstep time changes. Since the ankle and hip strategies have the same principle of regulating the reference point of COM divergence, the hip strategy is not implemented for faster implementation. This is done by setting both the upper and lower bounds of $\ddot{\theta}_{roll}$ and $\ddot{\theta}_{pitch}$ to zero.

The last graph of Fig. 8 presents the solve time while the robot responds to the disturbance. Since the framework solves the NMPC problem, it is necessary to ensure that the overall controller runs under real-time conditions. The average solve time of the proposed controller is 1.248×10^{-4} s, which is less than the sampling time of 0.002 s, and no cases violate the real-time condition.

Additionally, side-push recovery and walking on debris experiments are also performed to demonstrate the capability and practicality of the proposed method in more complex locomotion tasks (please see the supplementary video).

VI. Conclusion

This study proposed an NMPC algorithm to overcome the DCM error between the pre-defined gait pattern using various strategies that include ankle, hip, and stepping (footstep position and footstep time changes) strategies. Through the seamless consideration of these strategies, the proposed framework's push recovery performance was improved compared to the previous sequential approach in a simulation environment. Additionally, for the flexible application of the proposed controller, the point foot bipedal robot, which cannot utilize the ankle strategy, was balanced and overcame the disturbance while walking. The proposed method and its real-time performance were also verified with an experiment with an actual bipedal robot.

References

[1] H.-W. Park, A. Ramezani, and J. W. Grizzle, "A finite-state machine for accommodating unexpected large ground-height variations in bipedal robot walking," *IEEE Transactions on Robotics*, vol. 29, no. 2, pp. 331–345, 2012.

[2] S. Kajita and K. Tani, "Study of dynamic biped locomotion on rugged terrain-derivation and application of the linear inverted pendulum mode," in *IEEE International Conference on Robotics and Automation*, 1991, pp. 1405–1406.

[3] D. Kim *et al.*, "Dynamic locomotion for passive-ankle biped robots and humanoids using whole-body locomotion control," *International Journal of Robotics Research*, vol. 39, no. 8, pp. 936–956, 2020.

[4] B. E. Maki and W. E. McIlroy, "The role of limb movements in maintaining upright stance: the change-in-support strategy," *Physical Therapy*, vol. 77, no. 5, pp. 488–507, 1997.

[5] L. M. Nashner and G. McCollum, "The organization of human postural movements: a formal basis and experimental synthesis," *Behavioral and Brain Sciences*, vol. 8, no. 1, pp. 135–150, 1985.

[6] F. B. Horak and L. M. Nashner, "Central programming of postural movements: adaptation to altered support-surface configurations," *Journal of Neurophysiology*, vol. 55, no. 6, pp. 1369–1381, 1986.

[7] P.-B. Wieber, "Trajectory free linear model predictive control for stable walking in the presence of strong perturbations," in *IEEE-RAS International Conference on Humanoid Robots*, 2006, pp. 137–142.

[8] F. Nazemi, A. Yousefi-Koma, F. A.shirazi, and M. Khadiv, "A reactive and efficient walking pattern generator for robust bipedal locomotion," in *IEEE/RSJ International Conference on Robotics and Mechatronics*, 2017, pp. 364–369.

[9] H. Jeong *et al.*, "A robust walking controller based on online optimization of ankle, hip, and stepping strategies," *IEEE Transactions on Robotics*, vol. 35, no. 6, pp. 1367–1386, 2019.

[10] Z. Aftab, T. Robert, and P.-B. Wieber, "Ankle, hip and stepping strategies for humanoid balance recovery with a single model predictive control scheme," in *IEEE-RAS International Conference on Humanoid Robots*, 2012, pp. 159–164.

[11] H.-M. Joe and J.-H. Oh, "Balance recovery through model predictive control based on capture point dynamics for biped walking robot," *Robotics and Autonomous Systems*, vol. 105, pp. 1–10, 2018.

[12] J. Ding *et al.*, "Versatile reactive bipedal locomotion planning through hierarchical optimization," in *IEEE International Conference on Robotics and Automation*, 2019, pp. 256–262.

[13] J. Ding, S. Xin, T. L. Lam, and S. Vijayakumar, "Versatile locomotion by integrating ankle, hip, stepping, and height variation strategies," in *IEEE International Conference on Robotics and Automation*, 2021, pp. 2957–2963.

[14] J. Pratt, J. Carff, S. Drakunov, and A. Goswami, "Capture point: A step toward humanoid push recovery," in *IEEE-RAS International Conference on Humanoid Robots*, 2006, pp. 200–207.

[15] J. Englsberger, C. Ott, and A. Albu-Schäffer, "Three-dimensional bipedal walking control based on divergent component of motion," *IEEE Transactions on Robotics*, vol. 31, no. 2, pp. 355–368, 2015.

[16] M. Khadiv, A. Herzog, S. A. A. Moosavian, and L. Righetti, "Walking control based on step timing adaptation," *IEEE Transactions on Robotics*, vol. 36, no. 3, pp. 629–643, 2020.

[17] Y. Kojio *et al.*, "Footstep modification including step time and angular momentum under disturbances on sparse footholds," *IEEE Robotics and Automation Letters*, vol. 5, no. 3, pp. 4907–4914, 2020.

[18] S. Sato *et al.*, "Robust humanoid walking system considering recognized terrain and robots' balance," in *IEEE/RSJ International Conference on Intelligent Robots and Systems*, 2022, pp. 8298–8305.

[19] G. Mesesan, J. Englsberger, and C. Ott, "Online DCM trajectory adaptation for push and stumble recovery during humanoid locomotion," in *IEEE International Conference on Robotics and Automation*, 2021, pp. 12 780–12 786.

[20] R. Schuller *et al.*, "Online centroidal angular momentum reference generation and motion optimization for humanoid push recovery," *IEEE Robotics and Automation Letters*, vol. 6, no. 3, pp. 5689–5696, 2021.

[21] ——, "Online learning of centroidal angular momentum towards enhancing DCM-based locomotion," in *IEEE International Conference on Robotics and Automation*, 2022, pp. 10 442–10 448.

[22] M. B. Popovic, A. Goswami, and H. Herr, "Ground reference points in legged locomotion: Definitions, biological trajectories and control implications," *International Journal of Robotics Research*, vol. 24, no. 12, pp. 1013–1032, 2005.

[23] A. L. Hof, "The extrapolated center of mass concept suggests a simple control of balance in walking," *Human Movement Science*, vol. 27, no. 1, pp. 112–125, 2008.

[24] H. Jeong *et al.*, "Biped walking stabilization based on foot placement control using capture point feedback," in *IEEE/RSJ International Conference on Intelligent Robots and Systems*, 2017, pp. 5263–5269.

[25] S. Kajita *et al.*, "Biped walking pattern generation by using preview control of zero-moment point," in *IEEE International Conference on Robotics and Automation*, vol. 2, 2003, pp. 1620–1626.

[26] A. G. Pandala, Y. Ding, and H.-W. Park, "qpSWIFT: A real-time sparse quadratic program solver for robotic applications," *IEEE Robotics and Automation Letters*, vol. 4, no. 4, pp. 3355–3362, 2019.

[27] J. A. E. Andersson *et al.*, "CasADi – A software framework for nonlinear optimization and optimal control," *Mathematical Programming Computation*, vol. 11, no. 1, pp. 1–36, 2019.

[28] S. Hong, J.-H. Kim, and H.-W. Park, "Real-time constrained nonlinear model predictive control on SO(3) for dynamic legged locomotion," in *IEEE/RSJ International Conference on Intelligent Robots and Systems*, 2020, pp. 3982–3989.

[29] H. Jeong *et al.*, "Design and control of the rapid legged platform gazelle," *Mechatronics*, vol. 66, p. 102319, 2020.

[30] S. Kajita *et al.*, "Biped walking stabilization based on linear inverted pendulum tracking," in *IEEE/RSJ International Conference on Intelligent Robots and Systems*, 2010, pp. 4489–4496.